Reentrant phase transitions in threshold driven contagion on multiplex networks

Samuel Unicomb,[1,*] Gerardo Iñiguez,[2,3,4,†] János Kertész,[2,‡] and Márton Karsai [1,2,§]

[1]*Université de Lyon, ENS de Lyon, INRIA, CNRS, UMR 5668, IXXI, F-69364 Lyon, France*
[2]*Department of Network and Data Science, Central European University, H-1051 Budapest, Hungary*
[3]*Department of Computer Science, Aalto University School of Science, FIN-00076 Aalto, Finland*
[4]*IIMAS, Universidad Nacional Autonóma de México, 01000 Ciudad de México, Mexico*

Models of threshold driven contagion explain the cascading spread of information, behavior, systemic risk, and epidemics on social, financial, and biological networks. At odds with empirical observations, these models predict that single-layer unweighted networks become resistant to global cascades after reaching sufficient connectivity. We investigate threshold driven contagion on weight heterogeneous multiplex networks and show that they can remain susceptible to global cascades at any level of connectivity, and with increasing edge density pass through alternating phases of stability and instability in the form of reentrant phase transitions of contagion. Our results provide a theoretical explanation for the observation of large-scale contagion in highly connected but heterogeneous networks.

Information-communication technology has radically transformed social and economic interactions [1], introducing new means of transmitting ideas, behavior, and innovation [2,3], and overcoming limitations imposed by time and cognitive constraints [4,5]. The same technology provides an increasingly accurate picture of human interactions, mapping the underlying network structures that mediate dynamical processes, such as epidemics [6,7]. In complex contagion [3], characteristic of the spreading of innovation, rumors, or systemic risk, transmission is a collective phenomenon in which all social ties of an individual may be involved. The node degree, or number of links, is therefore critical to the dynamical outcome [8]; a large relative neighbor influence is easier to achieve the smaller the ego network. This behavior is well captured by threshold models of social contagion on single-layer unweighted networks, which predict large-scale cascades of adoption in relatively sparse networks [8–12]. In empirical social networks, however, individuals can maintain hundreds of ties [5,13], with interaction strength varying across social contexts [14–16], yet still exhibit frequent system-wide cascades of social contagion [17–21].

We address this issue by incorporating the relevant features of empirical social networks into a conventional threshold model. We consider that network ties are heterogeneous, and can be characterized by edge "types." In the case of social networks, these edge types vary in "quality" [22,23], usually associated with the intimacy or perceived importance of a relationship between individuals [24], and scale with the strength of interpersonal influence [25,26]. Heterogeneity in tie quality is well modeled by multiplex structures, as has been recognized in both network [27,28] and social science [29,30],

particularly regarding social contagion [31–34]. In multiplex models of social networks, individual layers represent the social context of a relationship (e.g., kinship, acquaintance), allowing us to classify ties by social closeness, as recognized by Dunbar's intimacy circle theory [24]. According to this theory, due to cognitive and time resources being finite but necessary to maintaining social ties, individuals actively cultivate a limited number of relationships, organizing them into intimacy circles that increase in size as they decrease in importance. Ego networks thus comprise a small but high-intimacy circle of close relationships, such as family and long-term friends, followed by large but low-intimacy circles of distant friends and acquaintances. Empirical evidence shows the distribution of dyadic social commitments (number of interactions or time devoted to peers) to be strongly heterogeneous [35,36]. Strikingly, this inverse relation between the cost of maintaining an edge type, and the abundance of that edge type, can be seen as an entropy maximization process [37] that applies to any system with a heterogeneous cost of edge formation and finite node resources. As such, although we use the language of social networks, our results are of relevance to other systems, e.g., financial [38–40] and biological [6,7] contagion.

Using analytical and numerical tools, we show that layer hierarchy can lead to global cascades in multiplexes with an average degree in the hundreds or thousands, perturbed by a single initial adoption. We report the observation that in a multiplex network with increasing link density a sequence of phase transitions occurs, resulting in alternating phases of stability and instability to global cascades.

Our model builds upon previous studies of threshold driven processes [8–11] and multiplex networks [27,28]. We define contagion as a binary-state dynamics over a weighted, undirected multiplex network of N nodes connected throughout M layers (Fig. 1). A node represents an individual u, and layer i the social context in which individuals interact, $1 \leqslant i \leqslant M$. The degree of u in each layer i takes discrete values $k_i = 0, \ldots, N-1$ according to the degree distribution $P_i(k)$. Edge

*samuelunicomb@gmail.com
†iniguezg@ceu.edu
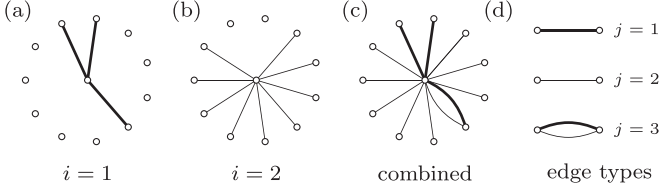‡kerteszj@ceu.edu
§marton.karsai@ens-lyon.fr

FIG. 1. (a), (b) Egocentric view of a multiplex structure with $M = 2$ layers, where edge density increases ($\delta_z > 1$) and edge weight decreases ($\delta_w < 1$) in each layer i. (c) Egocentric network overlap between layers. (d) Emergent edge types in the overlapping network. In the multiplex, the central node has a degree vector $\mathbf{k} = (2, 8, 1)^T$, encoding layer overlap.

weights $w_i(u, v)$ follow the continuous distribution $P_i(w)$ and capture the total capacity of nodes u and v to influence each other via layer i. The network allows for layer overlap [41] as nodes may be connected in multiple layers, modeling individuals who share several social contexts [Fig. 1(c)]. For simplicity, we assume that node degree is independent across layers, and that degree and weight distributions $P_i(k)$ and $P_i(w)$ differ by layer explicitly in their means $z_i = \sum_k k P_i(k)$ and $w_i = \int w P_i(w) dw$, but otherwise retain their functional form. In order to reproduce the hierarchical organization of edges suggested by intimacy circle theory [24], we assume that the mean degree z_i and weight w_i scale with layer index i as

$$z_{i+1} = \delta_z z_i \quad \text{and} \quad w_{i+1} = \delta_w w_i, \tag{1}$$

with $\delta_z \geqslant 1$ and $\delta_w \leqslant 1$. In other words, ego networks comprise a small number of high-intimacy neighbors [Fig. 1(a)] and a larger number of low-intimacy neighbors [Fig. 1(b)]. We fix the average total degree $z = \sum_i z_i$ as well as δ_z, which determines z_i. We also impose the arbitrary constraint $\langle w \rangle = 1$ and fix δ_w, which determines w_i (see Supplemental Material (SM) [42]).

In a binary-state model of contagion, nodes are in one of two mutually exclusive states, susceptible or infected (also called adopter or activated in the social contagion literature). Since nodes must be either connected or disconnected via each of the M network layers, their interaction is characterized by one of $2^M - 1$ resultant edge types [Fig. 1(d)], disregarding nodes disconnected in all layers, and indexing by j such that $1 \leqslant j \leqslant 2^M - 1$. Node configuration is thus described by the number of neighbors k_j and infected neighbors m_j across edges of type j, with $0 \leqslant m_j \leqslant k_j$. We store k_j and m_j in the degree vector $\mathbf{k}$ and partial degree vector $\mathbf{m}$, respectively (of dimension $2^M - 1$). Note that we consistently index the layer by i and the resultant edge type by j.

The threshold rule proposed by Watts [8–11] defines the fraction ϕ of neighbors that must be infected for a susceptible ego to adopt. This rule can be extended to multiplex networks in several ways (Table I). Denoting the set of neighbors of node u in layer i by $\mathcal{N}_i(u)$, the total influence upon u in layer i is $q_{k_i} = \sum_{v \in \mathcal{N}_i(u)} w_i(u, v)$. Restricted to infected neighbors $\mathcal{N}_i(u)|_I$, this gives $q_{m_i} = \sum_{v \in \mathcal{N}_i(u)|_I} w_i(u, v)$. In one variant of the threshold rule, nodes perceive influence in aggregate, summed over layers (reminiscent of neural networks [43,44]) and adopt with respect to a single threshold if $q_m \geqslant \phi q_k$,

TABLE I. Extensions of the Watts threshold rule to multiplex networks. Node state is determined by a single threshold ϕ and a weighted sum of influence over layers, or by individual layer thresholds ϕ_i and influence within each layer. In the former, the multiplex can be projected to a single weighted layer without loss of information relevant to the dynamics.

Weighted sum	Multiplex *or*	Multiplex *and*
$q_m \geqslant \phi q_k$	$\exists i$ s.t. $q_{m_i} \geqslant \phi_i q_{k_i}$	$q_{m_i} \geqslant \phi_i q_{k_i} \quad \forall i$

where $q_k = \sum_i q_{k_i}$ and $q_m = \sum_i q_{m_i}$ (weighted sum rule). In another variant, the node state is determined by M layer thresholds ϕ_i, along with influence q_{k_i} and q_{m_i} within layers. A node activates when $q_{m_i} \geqslant \phi_i q_{k_i}$ in every layer (multiplex *and* rule by Lee [33]), or in at least one layer (multiplex *or* rule [33]). Our aim is to show that multiplex networks following the structure of intimacy circle theory exhibit reentrant phase transitions for both the weighted sum and the multiplex *or* threshold rules. Note that if weights are uniform within each layer and the node state is determined by decisions within layers (*and* and *or* rules), then the structure is effectively unweighted. We show that even with this loss of weight information, reentrant phase transitions can still emerge due to contagion within layers.

We solve for our model using the approximate master equation (AME) formalism [45,46]. Similar to earlier solutions [10,15,17], at time t, the density of infected nodes ρ and the average probability ν_j that a j-type neighbor of a susceptible node is infected are governed by the system of coupled differential equations,

$$\begin{aligned} \dot{\nu}_j &= g_j(\boldsymbol{\nu}, t) - \nu_j, \\ \dot{\rho} &= h(\boldsymbol{\nu}, t) - \rho, \end{aligned} \tag{2}$$

where $g_j(\boldsymbol{\nu}, t)$ and $h(\boldsymbol{\nu}, t)$ are known functions (see SM and Ref. [15]). A numerical solution of Eq. (2) provides the dynamical evolution of each threshold rule, and linear stability analysis (LSA) [47] the region in (ϕ, z) space allowing global cascades (dashed-dotted lines in Figs. 2 and 3; shaded intervals in Fig. 4) (further details in SM). We derive a global cascade condition via the Jacobian matrix $\mathbf{J}$ corresponding to Eq. (2), evaluated at the fixed point $\boldsymbol{\nu}^* = \mathbf{0}$,

$$J_{ij}^* = -\delta_{ij} + \left. \frac{\partial g_i(\boldsymbol{\nu})}{\partial \nu_j} \right|_{\boldsymbol{\nu} = \boldsymbol{\nu}^*}, \tag{3}$$

which has eigenvalues λ_j. Global cascades occur if $\mathrm{Re}(\lambda_j) > 0$ for any $j = 1, \ldots, 2^M - 1$. In what follows we study the response of the network to an infinitesimal perturbation, or single infected seed, and record the relative frequency f_g of global cascades via Monte Carlo (MC) simulations. Regions in (ϕ, z) space with nonzero f_g in the $N \to \infty$ limit are well predicted by the spectrum of Eq. (3). For simplicity we assume uniform edge weights with value w_i within layers, which can be easily generalized (see SM).

The weighted sum rule leads to a high-z cascading phase, and thus reentrant phase transitions for constant ϕ, in an $M = 2$ layer multiplex with a log-normal (LN) degree distribution in each layer (Fig. 2, distribution details in SM). In two layers,
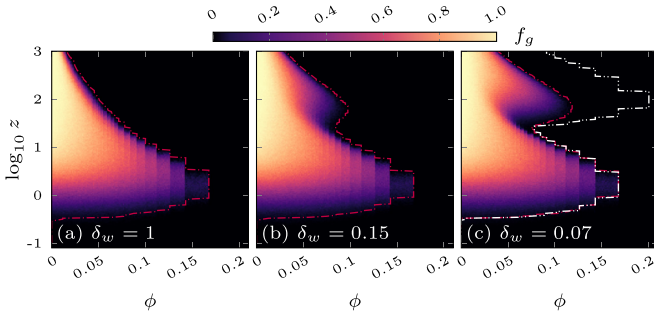
FIG. 2. Emergence of a high-z cascading phase in (ϕ, z) space for the weighted sum rule, for LN degree distribution, fixed $\delta_z = 50$, $\gamma = 0.5$, and decreasing δ_w. The standard deviation of the LN distribution is $\sigma_{k_i} = 2z_i$. MC simulations provide the relative frequency f_g of global cascades, after 10^3 instances of single node perturbation, in a configuration-model multiplex with $N = 10^6$. In (a) we recover the classic Watts phase diagram ($\delta_w = 1$). The constraint $\langle w \rangle = 1$ means $\mathbf{w} = (1, 1)^T$, $(6, 0.9)^T$, and $(11, 0.8)^T$, in panels (a), (b) and (c). The outer contour (dashed-double-dotted white line) in (c) shows the case $\delta_w \to 0$ [$\delta_w = 10^{-3}$; see heat map in Fig. 3(a)]. Dashed-dotted red lines show agreement with LSA prediction.

we define layer overlap as $\gamma = |E_1 \cap E_2|/|E_1|$, where E_i is the edge set in layer $i = 1, 2$ ($|E_1| < |E_2|$). We can increase weight heterogeneity by decreasing the weight scaling factor δ_w, resulting in a second cascading regime. As explained in Ref. [8], global cascades are due to "vulnerable" nodes with threshold sufficiently low that a single neighbor can infect them. A cascading phase is formed in (ϕ, z) space when vulnerable nodes form a percolating cluster. In single-layer unweighted networks, large z results in most nodes being stable against neighbor infection, and cascades becoming exponentially rare. However, under the weighted sum rule, weight heterogeneity allows one high-influence infected neighbor to dominate a node's total received influence if remaining neighbors have low influence. Crucially, such configurations are abundant when the conditions $\delta_z > 1$ and $\delta_w < 1$ are satisfied simultaneously, resulting in a percolating vulnerable cluster at high z. In the low-z phase, cascades are mediated by the connectivity of the weak layer, since the strong layer is too sparse to percolate. In the high-z phase, strong edges percolate and determine the stability of adjacent nodes that are otherwise stable to the dense weak layer. Both regions are accurately predicted by LSA [see Fig. 2 and velocity field analysis of Eq. (2) in SM]. Note that other mechanisms are able to generate additional transitions in (ϕ, z) space (e.g., degree assortativity in Ref. [34]).

We compare the behavior induced by the threshold rules of Table I for configuration-model multiplexes with LN degree distributions and a real-world multiplex extracted from Twitter (TW) (Fig. 3). TW comprises a sparse, strongly interacting layer ($z_1 = 5.4$) formed by mutual-mention interactions between $N = 3.7 \times 10^5$ users, and a dense layer of weak links ($z_2 = 163$) formed by the follower network of the same users. The two layers (taken as undirected; data details in SM) exhibit an overlap $\gamma = 0.45$. In order to explore the effect of single node perturbation over (ϕ, z) space, we remove edges uniformly at random from TW, decreasing its average degree z below its observed value of 165.8 [dashed lines in Figs. 3(d)–
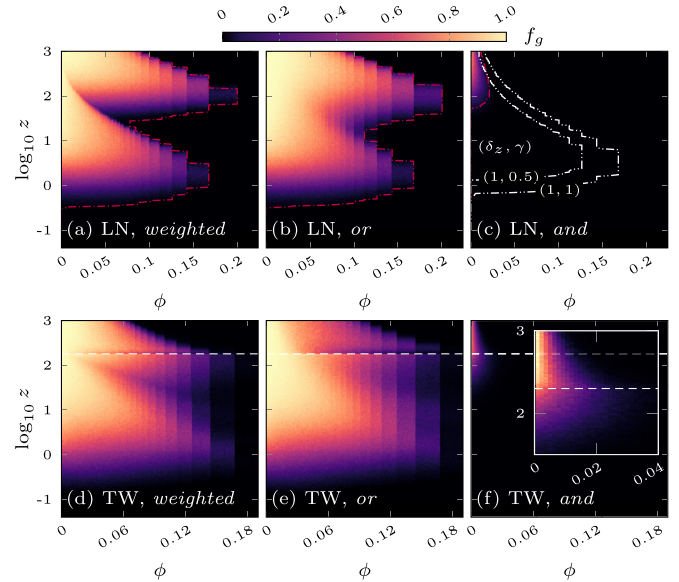

FIG. 3. Relative frequency f_g of global cascades in LN (top) and TW (bottom) multiplexes with $M = 2$ layers. LN networks in (a)–(c) are synthetic (standard deviation $\sigma_{k_i} = 2z_i$, overlap $\gamma = 0.5$, and density scaling $\delta_z = 50$). (a) Maximal weight heterogeneity ($\delta_w = 10^{-3}$) leads to reentrant transitions in the weighted sum rule. (b) Reentrant phase transitions also appear for the *or* threshold rule. (c) Under the *and* rule only one global cascading phase emerges, which vanishes when $\gamma = 0$. Decreasing δ_z and increasing γ expands the region of susceptibility to global cascades. See the outer dashed-double-dotted white contours (the LSA solution for $\delta_z = 1$, with $\gamma = 0.5$ and 1). (d)–(f) Reentrant phase transitions under the weighted sum and *or* rules in an empirical Twitter network ($\delta_z = 30.2$ and $\gamma = 0.45$). The dashed horizontal line at $z = 166$ is the empirical density, with sparsification providing lower z values, and densification higher z (see SM). (f) A single phase region observed in the *and* multiplex rule. LN and TW networks have size $N = 10^5$ and $N = 3.7 \times 10^5$. We obtain f_g via 10^3 realizations of single node perturbation. Dashed-dotted red lines show the LSA prediction.

3(f)]. Conversely, we use a model of network densification known as the forest-fire process [48] to extrapolate to higher z values (details in SM).

Assuming the weighted sum threshold rule [Figs. 3(a) and 3(d)], we find reentrant cascading phases under maximal weight heterogeneity ($\delta_w = 10^{-3}$) [for the approach to maximal heterogeneity see Figs. 2(a)–2(c) for LN, and SM for TW]. The multiplex *or* condition also leads to reentrant transitions in both LN and TW networks [Figs. 3(b) and 3(e)]. The onset of the high-z cascading phase, and thus of the reentrant transition, is triggered by the structural percolation of the sparse layer. Since the *or* rule considers influence within layers, and $P_i(w)$ is uniform here, the structure is effectively unweighted, underlining that density skewness is sufficient to trigger a reentrant phase when thresholds are layered. For both LN and TW networks, overlap γ and density skewness δ_z determine the stability under the *and* threshold rule [Figs. 3(c) and 3(f)]. Being the most restrictive condition, the *and* rule suppresses reentrant phase transitions and confines global cascades to a single phase at low ϕ, with cascades vanishing when $\gamma = 0$. As δ_z decreases and γ increases [Fig. 3(c)],
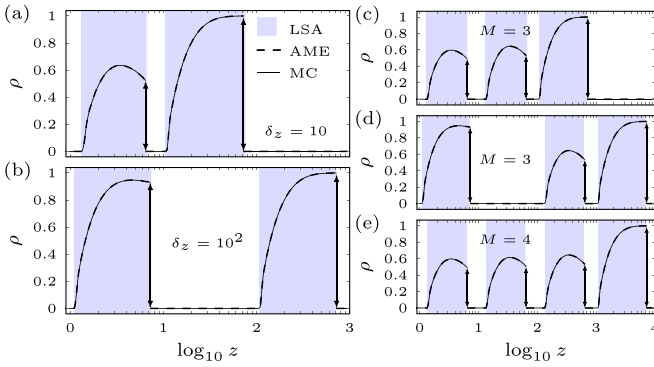
FIG. 4. Steady-state global cascade size as a function of average degree z, for constant threshold $\phi = 0.15$ and maximal weight heterogeneity ($\delta_w = 10^{-6}$), using the weighted sum rule. Degree distributions are Poissonian and the overlap is $\gamma = 0$. Shaded intervals due to LSA indicate systems with a positive leading eigenvalue (see SM); dashed lines indicate the steady-state solution of Eq. (2); and MC solutions are given by the solid curve (error bars narrower than the linewidth). (a), (b) Increasing density skewness δ_z delays the onset of high-z phases of contagion, and allows larger cascades in low-z phases in an $M = 2$ layer multiplex. (c)–(e) Increasing the number of layers to $M = 3$ and 4 induces 6 and 8 phase transitions in cascade size, respectively. (d) Varying δ_z, such that $z_2/z_1 = 100$, and $z_3/z_2 = 10$. MC results are averaged over 10^3 realizations of a single node perturbation, with $N = 10^7$.

overlapping edges, necessary for mediating cascades under the *and* rule, become more abundant and increase the area of the unstable phase [Fig. 3(c)]. For simplicity, we set $\phi_i = \phi$ for the *and* and *or* rules. Inspection of the contours of Figs. 3(a)–3(c) reveals that the weighted sum rule occupies an area intermediate between the *and* and *or* rules; we perform a comparative eigenvalue analysis in the SM to argue that this is generally the case.

We illustrate using the weighted sum rule that density skewness δ_z determines the average degree z at which reentrant phases are triggered [Figs. 4(a) and 4(b)]. This is because the structural percolation transition of individual layers is necessary for the percolation of a subgraph of vulnerable nodes; the value of z at which this occurs depends on δ_z. Increasing

the number of layers in the network also creates additional phases of contagion [see Figs. 4(c)–4(e) for $M = 3$, 4]. When δ_z differs between layers, the onset of contagion phases may be delayed or promoted [Fig. 4(d)]. In lower phases, strong edges that are too sparse to percolate structurally inhibit cascades driven by edges that are denser but weaker, leading to "partial" cascades that are global but do not fill the network [e.g., lower phase in Fig. 4(a)]. This is due to the immunizing effect of strong edges in information diffusion; pairs of susceptible nodes connected by a sufficiently strong edge are impossible to infect if all other neighbors are weak, even if all those weak neighbors are infected. These configurations are abundant when the strong layer is yet to undergo structural percolation.

Our results demonstrate that global information cascades emerge in arbitrarily dense networked systems, typically viewed as stable against small perturbations. The types of multiplex structure triggering this behavior are elementary, and have even been derived from an entropy maximization process. We have shown that skewness in edge density by layer is necessary for the emergence of reentrant phase transitions under all variants of the threshold rule, but sufficient only when thresholds are layered and the *or* rule applied. When influence is summed over layers and evaluated with respect to a single threshold, an additional weight skewness condition is necessary. We confirm these phenomena using an analytical formalism that we have extended to multiplex networks, as well as simulation, both on synthetic networks and an empirical Twitter multiplex where all results are recovered. Our results suggest approaches to network design that may promote or suppress system-wide cascades of threshold driven contagion.

[1] J. Borge-Holthoefer, R. A. Baños, S. González-Bailón, and Y. Moreno, J. Complex Networks **1**, 3 (2013).

[2] E. M. Rogers, *Diffusion of Innovations* (Simon and Schuster, New York, 2010).

[3] D. Centola and M. Macy, Am. J. Sociol. **113**, 702 (2007).

[4] R. I. Dunbar, J. Human Evol. **22**, 469 (1992).

[5] B. Gonçalves, N. Perra, and A. Vespignani, PLoS One **6**, e22656 (2011).

[6] R. I. Joh, H. Wang, H. Weiss, and J. S. Weitz, Bull. Math. Biol. **71**, 845 (2009).

[7] T. Takaguchi, N. Masuda, and P. Holme, PLoS One **8**, e68629 (2013).

[8] D. J. Watts, Proc. Natl. Acad. Sci. USA **99**, 5766 (2002).

[9] M. Granovetter, Am. J. Sociol. **83**, 1420 (1978).

[10] Z. Ruan, G. Iñiguez, M. Karsai, and J. Kertész, Phys. Rev. Lett. **115**, 218702 (2015).

[11] P. D. Karampourniotis, S. Sreenivasan, B. K. Szymanski, and G. Korniss, PLoS One **10**, e0143020 (2015).

[12] M. Karsai, G. Iñiguez, K. Kaski, and J. Kertész, J. R. Soc. Interface **11**, 20140694 (2014).

[13] R. I. Dunbar, Philos. Trans. R. Soc., B **367**, 2192 (2012).

[14] H.-H. Jo, Y. Murase, J. Török, J. Kertész, and K. Kaski, Physica A **500**, 23 (2018).

[15] S. Unicomb, G. Iñiguez, and M. Karsai, Sci. Rep. **8**, 3094 (2018).

[16] R. Burkholz, A. Garas, and F. Schweitzer, Phys. Rev. E **93**, 042313 (2016).

[17] M. Karsai, G. Iñiguez, R. Kikas, K. Kaski, and J. Kertész, Sci. Rep. **6**, 27178 (2016).

[18] E. Bakshy, J. M. Hofman, W. A. Mason, and D. J. Watts, in *Proceedings of the Fifth International AAAI Conference on Weblogs and Social Media (ICWSM)* (AAAI Press, Menlo Park, CA, 2011), pp. 65–74.

[19] J. Ugander, L. Backstrom, C. Marlow, and J. Kleinberg, Proc. Natl. Acad. Sci. USA **109**, 5962 (2012).

[20] P. A. Dow, L. A. Adamic, and A. Friggeri, ICWSM **1**, 12 (2013).

[21] J. P. Gleeson and R. Durrett, Nat. Commun. **8**, 1227 (2017).

[22] M. S. Granovetter, *Social Networks* (Elsevier, Amsterdam, 1977), pp. 347–367.

[23] I. Kawachi and L. F. Berkman, J. Urban Health **78**, 458 (2001).

[24] W.-X. Zhou, D. Sornette, R. A. Hill, and R. I. M. Dunbar, Proc. R. Soc. B: Biol. Sci. **272**, 439 (2005).

[25] R. B. Cialdini and N. J. Goldstein, Annu. Rev. Psychol. **55**, 591 (2004).

[26] J. C. Turner, *Social Influence* (Thomson Brooks/Cole, Belmont, 1991).

[27] M. Kivelä, A. Arenas, M. Barthelemy, J. P. Gleeson, Y. Moreno, and M. A. Porter, J. Complex Networks **2**, 203 (2014).

[28] S. Boccaletti, G. Bianconi, R. Criado, C. I. del Genio, J. Gómez-Gardeñes, M. Romance, I. Sendiña-Nadal, Z. Wang, and M. Zanin, Phys. Rep. **544**, 1 (2014).

[29] B. Kapferer, in *Social Networks in Urban Situations: Analyses of Personal Relationships in Central African Towns*, edited by J. C. Mitchell (Manchester University Press, Manchester, UK, 1969).

[30] L. M. Verbrugge, Social Forces **57**, 1286 (1979).

[31] O. Yağan and V. Gligor, Phys. Rev. E **86**, 036103 (2012).

[32] C. D. Brummitt, K.-M. Lee, and K.-I. Goh, Phys. Rev. E **85**, 045102(R) (2012).

[33] K. M. Lee, C. D. Brummitt, and K. I. Goh, Phys. Rev. E **90**, 062816 (2014).

[34] Y. Zhuang, A. Arenas, and O. Yağan, Phys. Rev. E **95**, 012312 (2017).

[35] P. V. Marsden and K. E. Campbell, Social Forces **63**, 482 (1984).

[36] J.-P. Onnela, J. Saramäki, J. Hyvönen, G. Szabó, D. Lazer, K. Kaski, J. Kertész, and A.-L. Barabási, Proc. Natl. Acad. Sci. USA **104**, 7332 (2007).

[37] I. Tamarit, J. A. Cuesta, R. I. Dunbar, and A. Sánchez, Proc. Natl. Acad. Sci. USA **115**, 8316 (2018).

[38] M. Elliott, B. Golub, and M. O. Jackson, Am. Econ. Rev. **104**, 3115 (2014).

[39] S. Battiston, D. Delli Gatti, M. Gallegati, B. Greenwald, and J. E. Stiglitz, J. Econ. Dyn. Control **36**, 1121 (2012).

[40] H. Amini, R. Cont, and A. Minca, Math. Finance **26**, 329 (2016).

[41] D. Cellai, E. López, J. Zhou, J. P. Gleeson, and G. Bianconi, Phys. Rev. E **88**, 052811 (2013).

[42] See Supplemental Material at http://link.aps.org/supplemental/10.1103/PhysRevE.100.040301 for additional information on analytical calculations, numerical simulations, and data analysis.

[43] W. Gerstner, W. M. Kistler, R. Naud, and L. Paninski, *Neuronal Dynamics: From Single Neurons to Networks and Models of Cognition* (Cambridge University Press, Cambridge, UK, 2014).

[44] R. Iyer, V. Menon, M. Buice, C. Koch, and S. Mihalas, PLoS Comput. Biol. **9**, e1003248 (2013).

[45] J. P. Gleeson, Phys. Rev. Lett. **107**, 068701 (2011).

[46] J. P. Gleeson, Phys. Rev. X **3**, 021004 (2013).

[47] M. A. Porter and J. P. Gleeson, Front. Appl. Dyn. Syst. Rev. Tutor. **4**, (2016).

[48] J. Leskovec, J. Kleinberg, and C. Faloutsos, ACM Trans. Knowl. Discovery Data **1**, 2 (2007).